NUCL SCI TECH (2022) 33:91
https://doi.org/10.1007/s41365-022-01066-2

Silicon PIN photodiode applied to acquire high-frequency sampling XAFS spectra

Yun-Peng Liu[1] · Lei Yao[1] · Bing-Jie Wang[1] · Jia-Jun Zhong[1,2] · Hao Wang[1,2] · Li-Xiong Qian[1,2] · Zhong-Jun Chen[1] · Guang Mo[1] · Xue-Qing Xing[1] · Wei-Fan Sheng[1,2] · Zhong-Hua Wu[1,2]

Received: 18 April 2022 / Revised: 8 June 2022 / Accepted: 9 June 2022 / Published online: 18 July 2022

Abstract Experimental techniques based on SR facilities have emerged with the development of synchrotron radiation (SR) sources. Accordingly, detector miniaturization has become significant for the development of SR experimental techniques. In this study, the miniaturization of a detector was achieved by coupling a commercial silicon PIN photodiode (SPPD) into a beamstop, aiming for it not only to acquire X-ray absorption fine structure (XAFS) spectra, but also to protect the subsequent two-dimensional detector from high-brilliance X-ray radiation damage in certain combination techniques. This mini SPPD detector coupled to a beamstop was used as the rear detector in both the conventional sampling scheme and novel high-frequency (HF) sampling scheme to collect the transmission XAFS spectra. Traditional ion chambers were also used to collect the transmission XAFS spectra, which were used as the reference. These XAFS spectra were quantitatively analyzed and compared; the results demonstrated that the XAFS spectra collected by this SPPD in both the conventional sampling scheme and HF sampling scheme are feasible. This study provides a new detector-selection scheme for the acquisition of the quick-scanning XAFS (QXAFS) and HF sampling XAFS spectra. The SPPD detector presented in this study can partially meet the requirements of detector miniaturization.

Keywords Silicon PIN photodiodes · Beamstop · XAFS · High frequency sampling

This work was supported by the National Key R&D Program of China (Nos. 2017YFA0403000 and 2017YFA0403100).

✉ Zhong-Hua Wu
wuzh@ihep.ac.cn

[1] Beijing Synchrotron Radiation Facility, Institute of High Energy Physics, Chinese Academy of Sciences, Beijing 100049, China

[2] University of Chinese Academy of Sciences, Chinese Academy of Sciences, Beijing 100049, China

1 Introduction

X-ray absorption fine structure [1–5] (XAFS) spectroscopy based on synchrotron radiation (SR) sources is a powerful tool for determining the electronic and atomic local structures, as well as the chemical-physical states of elements in condensed matter. The ion chamber (IC) is the most commonly used detector to collect XAFS signals, which exhibits a good linear response to the X-ray intensity for a wide range of energies [6]. However, a few drawbacks of IC include microphonic noise and the problematic electron–ion pair recombination [6, 7] enhanced by a high X-ray flux. Thus, finding a substitute for IC is desirable to accurately acquire a high-flux X-ray intensity. Silicon PIN photodiodes (SPPD) and diamond-based photodetectors (DD) were often used as substitutes for ion chambers and have been investigated for more than two decades. Sato [6] investigated the feasibility of SPPD as an X-ray intensity monitor and found that these detectors were adequately feasible for XAFS experiments because their spectra had nearly the same quality as that of IC, and it can be more effective than IC for a high X-ray flux. Dalba et al. [7] studied the properties of SPPD as X-ray detectors for Extended-XAFS (EXAFS) measurements and found that good-quality EXAFS measurements with SPPD were possible if diffraction effects were eliminated. Pace et al. [8] studied the application of DD to XAFS measurements between the energy range of 4–13 keV and found that all the XAFS spectra were significantly similar to the spectrum from IC and exhibited a good signal-to-noise ratio (SNR). De Sio et al. [9] performed a direct comparison between an IC and a nitrogen-doped single-crystal DD applied to Fe K-edge XAFS spectroscopy and found that the EXAFS data and parameter values obtained in the transmission mode by both the DD and a standard IC were in good agreement. Ravel et al. [10] evaluated the performance of DD as an incident beam monitor and verified that the effect of diffraction on XAFS measurements can be effectively eliminated if DD is combined with polycapillary lenses. Semiconductor-type detectors have the advantages [11] of a high response, no microphonic noise, good linearity, and a wide dynamic range. In particular, they make it easier to miniaturize detectors to a sufficiently small size. In addition to the limitations of the traditional IC used in high-flux X-ray detection, its large size limits its application [12–15] in certain combined detection techniques. Small-sized SPPD and DD may be more advantageous for high-flux XAFS measurements in certain combination techniques.

Compared to DD, SPPD is more economical and easier to obtain from commercial markets. Blanchet et al. [16] developed a small and robust SPPD built into a beamstop for detecting backscattered X-ray photons, demonstrating a good response to X-ray intensity between the energy range of 6–20 keV. Beale et al. [12] also successfully obtained XAFS signals of the Zn K-edge using a photodiode in a combined small-angle X-ray scattering (SAXS)/wide-angle X-ray scattering (WAXS)/XAFS setup. Over the past few decades, several measurement approaches have been developed to reduce the time required to collect an entire XAFS spectrum. The Quick-scanning EXAFS (QEXAFS) technique [17, 18] not only dramatically reduced the data collection time of an entire EXAFS spectrum to a few seconds or less, but also maintained a high SNR [19] of the obtained QEXAFS spectrum. Yu et al. [20] developed a QEXAFS method with a time resolution of 2 s based on the EPICS and LabVIEW software at the BL14W1 beamline of the Shanghai Synchrotron Radiation Facility (SSRF). Khalid et al. [21] refined the QEXAFS technique. The QEXAFS spectrum acquisition time was reduced to milliseconds by driving the channel-cut Si(111) monochromator to oscillate at a frequency of 5 Hz with a tangential arm. In addition, the use of high-speed counting cards (HSCC) is also an effective method used to accelerate XAFS data collection; here, it was named the high-frequency (HF) sampling scheme. Using the IK220 HSCC card and IC, a similar HF sampling mode [22] has been reported. In a compact combined technique, SPPD is apparently more advantageous than IC owing to its small size. However, the afterglow effect and detection efficiency of SPPD can be disadvantageous [6] for rapid measurements. Therefore, SPPD may be considered less suitable for QEXAFS measurements than routine IC. Although previous studies have demonstrated that SPPD can be sufficiently used in the conventional XAFS collection, the feasibility of SPPD applied to acquire HF sampling XAFS spectra has not yet been studied, especially when the SPPD is coupled into the SAXS beamstop of a combining setup. This study aims to determine whether the SPPD used as a rear detector is comparable to the DD used as the front detector in the HF sampling scheme. If the small-sized SPPD can be used for HF-sampling XAFS measurements, it will be significantly beneficial to develop these combined techniques including XAFS measurements.

In this study, a commercial SPPD was coupled with a beamstop used in conventional SAXS measurements to protect the subsequent two-dimensional detector from irradiation damage. This beamstop-coupled SPPD obtains the role of a rear detector in transmission XAFS measurements. By comparing the performance of this miniaturized SPPD with those of DD and IC in transmission XAFS measurements, its feasibility and validity for acquiring the conventional and HF sampling XAFS spectra are discussed.

2 Preparation of silicon PIN photodiode

In a typical XAFS transmission mode, an ion chamber is used to monitor the X-ray intensity (I_0) in front of the sample, referred to as the XAFS front detector (FD). Another ion chamber was used to monitor the X-ray intensity (I_1) behind the sample, here named the XAFS rear detector (RD). For a sample with a thickness d, the absorption coefficient (μ) can be expressed as follows: $\mu(E)d = \ln(I_0/I_1)$. However, owing to the large size of the ion chamber, it is often difficult to meet the requirements of XAFS measurements using a combined technique involving an ion chamber. A transmission-type detector should generally be used to record the incident X-ray intensity; evidently, the SPPD is not suitable for I_0 detection in front of the sample. In this study, DD [23] or IC was used as the front detector for the XAFS measurement to detect the incident X-ray intensity (I_0). A mini SPPD was used as the rear detector to record the X-ray transmission intensity (I_1) behind the sample. To maintain a maximum distance of the rear detector used for XAFS measurements from other experimental signal paths, its size should be minimized. To optimize the coupling of a mini-SPPD into a beamstop, it is typically mounted in a vacuum tube for SAXS measurements and maintained at a distance from the sample to avoid blocking other experimental signals. This type of SPPD can not only be used for XAFS signal acquisition but can also prevent irradiation damage of the direct beam to the SAXS detector.

In this study, the SPPD was purchased from Beijing Lightsensing Technologies Ltd., as shown in Fig. 1a. The model used was LSSPD-SPB3; the effective photosensitive area was 3 × 3 mm^2. The maximum spectrum response at 940 nm was 0.5 A/W, which is larger than the previously reported 0.43 A/W [6] of S1227-1010BR SPPD at 720 nm. Other factory parameters for this SPPD are listed in Table 1. To achieve spatial compatibility for the simultaneous measurement of the SAXS, XRD, and XAFS signals, the SPPD was coupled into a beamstop with a volume of 12 × 6 × 6 mm^3. The beamstop was supported by a hollow cylindrical rod with an outer diameter of 3 mm, as shown in Fig. 1b. The beamstop had a rectangular opening, and the SPPD embedded in the beamstop faced the transmission beam behind the sample. Note, Kocsisa and Somogyi [24] developed a miniature IC for X-ray microprobe measurements at the European Synchrotron Radiation Facility (ESRF); however, this miniature IC was insufficiently small for SAXS/XRD/XAFS combined measurements. If the aforementioned miniature IC was to be used for recording the transmission X-ray intensity, it would need to be placed at the downstream end; otherwise, it would obscure the SAXS or XRD signal. In addition, its design, which lacks window material, contains dozens of

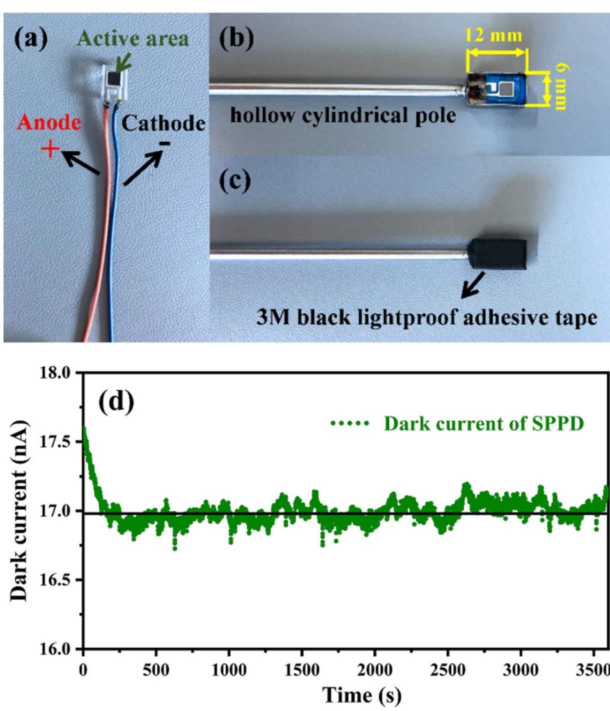

Fig. 1 (Color online) Photographs of **a** the purchased LSSPD-SPB3 SPPD, **b** SPPD embedded in a beamstop, and **c** beamstop wrapped with 3 M black lightproof adhesive tape. **d** Dark current of the SPPD embedded in the beamstop and wrapped with 3 M black lightproof adhesive tape

Table 1 Absolute maximum ratings and electrical and optical characteristic parameters of LSSPD-SPB3 SPPD (T = 25 °C)

Parameter	Value
Absolute maximum ratings	
Operating temperature, T_{op} (°C)	−25 ~ + 85
Storage temperature, T_{stg} (°C)	−40 ~ + 85
Forward current, I_f (mA)	10
Reverse current, I_r (μA)	1000
Soldering temperature (10 s), T_s (°C)	260
Parameter	Typical value
Electrical and optical characteristics (T = 25 °C)	
Spectral range, λ (nm)	300 ~ 1200
Responsivity	
$Re_{\lambda=1200\ nm}$ (mA/mW)	0.2
$Re_{\lambda=940\ nm}$ (mA/mW)	0.5
$Re_{\lambda=650\ nm}$ (mA/mW)	0.35
$Re_{\lambda=300\ nm}$ (mA/mW)	0.1
Operating voltage, V_R (V)	0 ~ 10
Dark current, I_D (V_R = 10 V) (nA)	5
Rise time, T_r (V_R = 10 V) (ns)	50

micron entrance pinholes, and has a constant Ar pressure flow of approximately 1 atm, will severely restrict its effectiveness in the SAXS/XRD/XAFS combined technique. Therefore, it is necessary to develop a mini SPPD detector for XAFS measurements in the SAXS/XRD/XAFS combined technique.

The SPPD is relatively sensitive to visible and infrared radiation. To avoid interference from signals other than X-rays, the SPPD must be kept at a distance from visible and infrared lights. Therefore, the SPPD was coupled into a beamstop and further wrapped with black 3 M tape, as shown in Fig. 1c. The dark current (I_{dark}) of the as-prepared SPPD was measured to be approximately 17 nA, as shown in Fig. 1d. Previous studies [25, 26] have demonstrated that the dark current I_{dark} consists of a bulk leakage current (I_{bulk}) and surface leakage current (I_{surf}). The former is proportional to the mesa area of the diode, whereas the latter is perimeter-dependent on the mesa sidewall; both originate from defects. A decrease of approximately 0.5 nA was noted in the dark current at the beginning when the dark current of the as-prepared SPPD detector was measured. This may be attributed to the small number of dangling bonds on the surface of the SPPD, which initially captured a certain amount of charge. When an external electric field was applied to the SPPD, these captured charges were gradually released and depleted, causing the dark current to decrease at the beginning and reach a quasi-equilibrium state. When the incident X-ray energy value was near the Cu K-edge, approximately 9 keV, the X-ray intensity was approximately 10^{12} cps at beamline 1W2B of the Beijing Synchrotron Radiation Facility (BSRF), which corresponds to an irradiation power of approximately 1.44 mW. The response current induced by the transmission beam was usually in the range of several hundreds of μA to a few mA when measuring the K-edge X-ray absorption spectra of the transition metals using this SPPD. Compared to the dark current of 17 nA, the dynamic range of this SPPD at nearly 9 keV was approximately 10^4–10^5. Theoretically, this SPPD can be sufficiently used for the K-edge XAFS measurements of transition metals.

3 XAFS data acquisition

The feasibility of this SPPD used for XAFS measurements was verified at beamline 1W2B of the BSRF. The storage ring was run at 2.5 GeV with an electron-beam current of approximately 250 mA. The X-ray energy range of beamline 1W2B was between 5 to 18 keV, which can be monochromized by a Si(111) monochromator with an energy resolution ($\Delta E/E$) of approximately 2×10^{-4}. The X-ray spot size was approximately 1.0 (H) × 0.5 (V) mm^2 at the sample position. The X-ray photon flux was approximately 1.0×10^{12} photons/s at the Cu K-edge (8979 eV). To assess the feasibility of the SPPD used for XAFS measurements, conventional K-edge XAFS spectra and HF sampling K-edge XAFS spectra of the standard Cu foil were collected. By replacing the detectors, three groups of detector combinations labeled FD-RD (including IC-IC, IC-SPPD, and DD-SPPD) were used in the conventional XAFS measurements, where FD represents the front detector (I_0) in front of the sample and RD represents the rear detector (I_1) behind the sample. When the DD was used as the front detector [23], the sensitive area was 10 × 10 mm^2. The thickness of the diamond film was 0.5 mm and a bias voltage of 300 V was applied to both sides of the diamond film. Because the large size of the ion chamber is unavoidable, the ion chamber is not considered in the HF sampling mode that is mainly used for the combined technique. Therefore, in the HF sampling XAFS measurements, only one group of detector combinations, labeled as DD-SPPD, was used to collect the XAFS spectra. The main difference between the conventional XAFS mode and the HF sampling XAFS mode was that the 974 counter was used in the conventional XAFS mode, whereas a high-speed counter card was used in the HF sampling XAFS mode. A schematic of the two sampling modes is illustrated in Fig. 2. For comparison, the XAFS spectra collected with different detector combinations were directly labeled as FD-RD, where the front detector (FD) was used to record the X-ray intensity (I_0) in front of the sample and the rear detector (RD) was used to record the X-ray intensity (I_1) behind the sample. All collected XAFS data were processed and analyzed using a comprehensive Demeter [27] program.

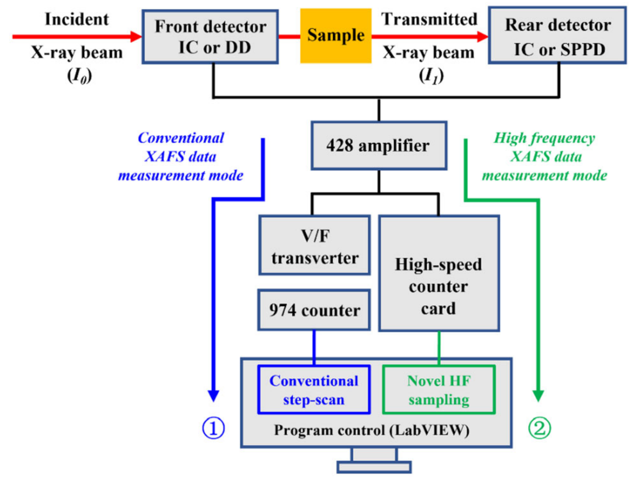

Fig. 2 Schematic diagram of conventional (route 1) and HF sampling (route 2) XAFS measurement modes

4 Results and discussion

4.1 Feasibility of SPPD for XAFS measurements

The Cu K-edge X-ray absorption spectrum of the Cu foil was first collected using the DD-SPPD detector combination in the conventional mode, as shown in Fig. 3a. As a reference, the Cu K-edge X-ray absorption spectrum of the Cu foil was then collected with the IC-IC detector combination in the conventional sampling mode, as shown in Fig. 3a. By comparing the two X-ray absorption spectra, it was found that the fine structures and oscillation amplitudes of IC-IC and DD-SPPD were nearly the same. Based on Fig. 3b, c, these two XAFS spectra are highly consistent both in the k-space and R-space, further confirming the consistency of the spectral characteristics collected by the two detector combinations of IC-IC and DD-SPPD. Furthermore, the repeatability of the XAFS data was verified by comparing three independent XAFS scans of the Cu foil Cu K-edge, as shown in Fig. 3d. From the three XAFS spectra repeatedly acquired using the DD-SPPD detector combination, the three Cu K-edge X-ray absorption spectra were found to be nearly the same, presenting excellent repeatability. This result indicates that in addition to the SPPD not being damaged by the continuous X-ray radiation, the XAFS data quality collected by the DD-SPPD detector combination was approximately the same as that collected by the widely used IC-IC detector combination. As indicated, the incident X-ray intensity was

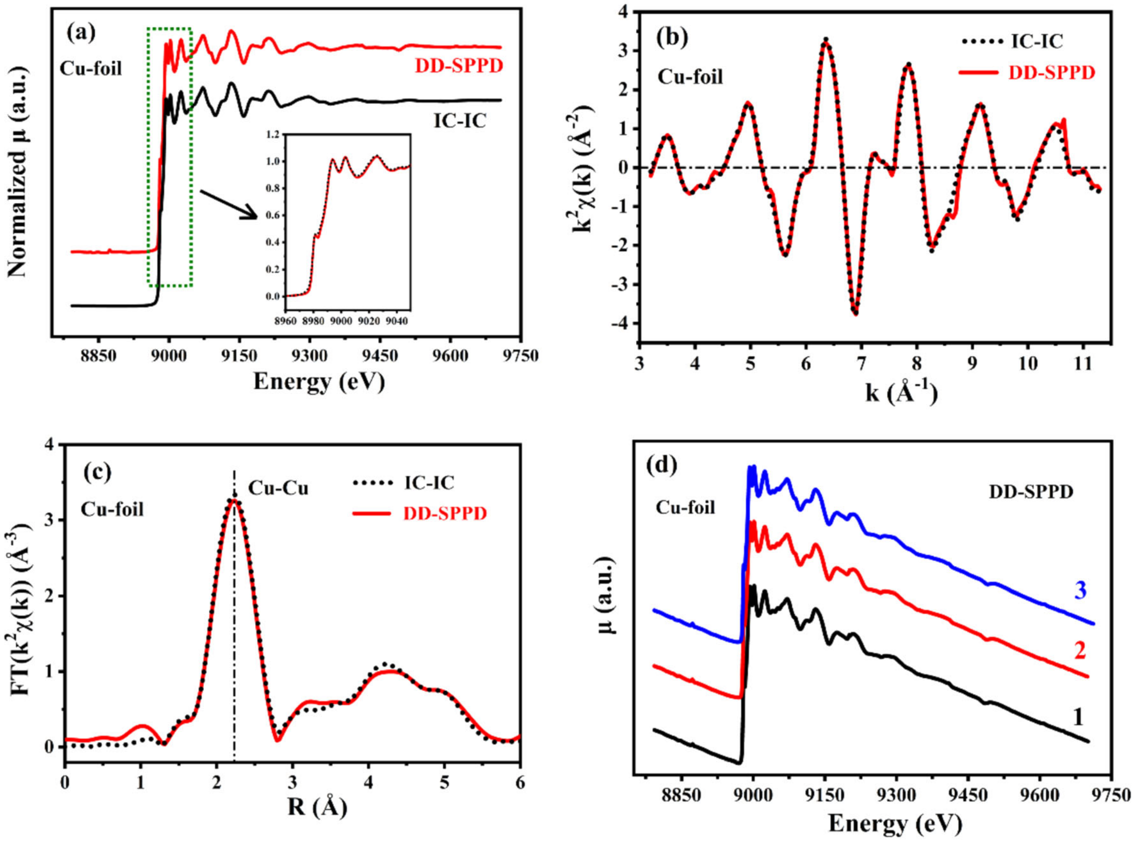

Fig. 3 (Color online) Cu K-edge XAFS spectra of Cu foil in *E*-space (**a**), *k*-space, (**b**) and *R*-space (**c**) collected by different combinations of front and rear detectors (IC-IC and DD-SPPD) with the conventional XAFS transmission mode. Three independent absorption spectra of Cu K-edge (**d**), confirming the repeatability of XAFS data collected by the SPPD

approximately 10^{12} cps in the Cu K-edge XAFS spectra measurements. As a conservative estimate, a total of 20 min were required for acquiring a complete XAFS spectrum in the conventional XAFS sampling mode or step scanning mode. The SPPD was continuously exposed to the transmission X-ray beam for tens of minutes in a single XAFS scan; whereas in the HF sampling mode, the continuous exposure time of the SPPD was only for a dozen seconds. The reproducibility of the XAFS spectral characteristics in the conventional XAFS measurements clearly indicates that irradiation damage did not occur in the SPPD, as it was used to record the XAFS signals. The lifetime of SPPD depends on the exposure time in addition to the irradiation dosage. Namely, this type of photodiode can be stably used for the collection of transmission XAFS data if the incident X-ray flux is not higher than 10^{12} cps. Based on these results, visible and infrared photodiodes can be sufficiently used for the acquisition of the transmission X-ray absorption spectra, verifying the feasibility of SPPD used for XAFS measurements.

4.2 Comparison of detector combinations

The aforementioned results confirm the feasibility of the DD-SPPD detector combination for conventional transmission XAFS measurements. The IC-SPPD detector combination was also used to collect the Cu K-edge X-ray absorption spectrum of the Cu foil, and the obtained XAFS spectrum was labeled IC-SPPD. For comparison, the conventional Cu K-edge XAFS spectrum of the Cu foil collected with the IC-IC detector combination was used as a reference. The three Cu K-edge X-ray absorption spectra of the Cu foil are shown in Fig. 4a, b. The three detector combinations can obtain nearly the same X-ray absorption spectra as that in the *E*-space or the XAFS curves in the *k*-space. Apparently, both DD and IC can be used as the front detectors when SPPD is used as the rear detector; the two-detector combinations of DD-SPPD and IC-SPPD are feasible for XAFS measurements.

To quantitatively evaluate the difference between the two XAFS curves, a deviation factor (Q) was defined as follows:

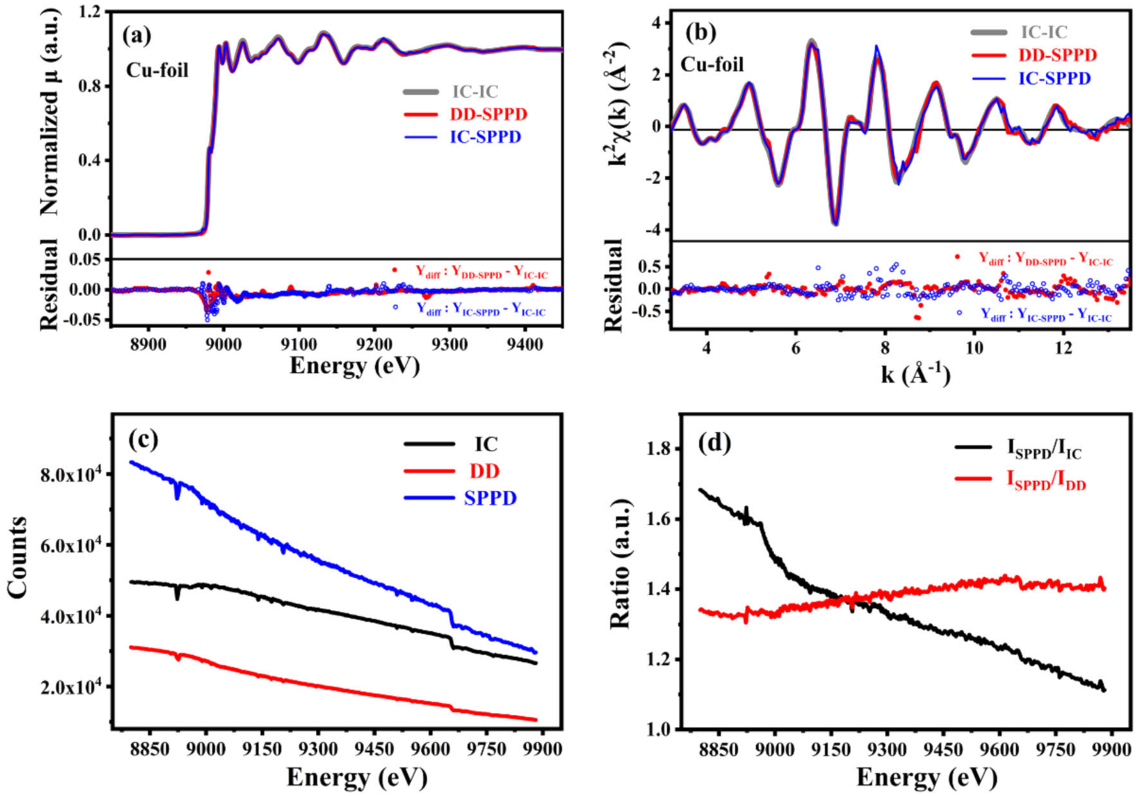

Fig. 4 (Color online) Cu K-edge XAFS spectra of Cu-foil in *E*-space (**a**) and *k*-space (**b**) collected with IC-IC, DD-SPPD, and IC-SPPD detector combinations in a conventional transmission mode as well as their differences. **c** The X-ray intensity responses at different energies recorded by the IC, DD, and SPPD detectors. **d** The intensity response ratios of SPPD to IC and SPPD to DD at different energies

$$Q = \sum_{i}^{N} |Y_i - Y_{0i}| / \sum_{i=1}^{N} |Y_{0i} - \overline{Y}_0|. \quad (1)$$

Here, Y_0, Y, and $\overline{Y}_0$ indicate the reference function, function to be estimated, and mean value of the reference function, respectively, N indicates the number of data points, and subscript i denotes the ith data point. The Q value calculated using Eq. (1) indicates the statistical average of the relative difference of a single data point between the curve to be estimated and the reference curve. A smaller Q value indicates a higher similarity between the two curves. After considering the possible errors, if the calculated Q value was less than 0.25, the two related curves were considered to be roughly the same. When the two curves were exactly the same, the Q value was equal to zero. Considering the data collected with the conventional IC-IC detector combination as the reference data, the calculated Q values for the three X-ray absorption curves shown in Fig. 4a are 0 (IC-IC), 0.024 (IC-SPPD), and 0.024 (DD-SPPD). The calculated Q values for the three XAFS curves shown in Fig. 4b are 0 (IC-IC), 0.121 (IC-SPPD), and 0.116 (DD-SPPD).

The calculated Q values demonstrate that the DD-SPPD and IC-SPPD detector combinations can acquire XAFS data closer to the reference data collected by the IC-IC detector combination; however, the IC-SPPD detector combination presents slight glitches on the XAFS spectrum compared to that collected by the IC-IC detector combination. This is because the IC and SPPD exhibited slightly different responses to the X-ray energy, as shown in Fig. 4c. Consequently, certain unnecessary and harmful glitches were not sufficiently removed and were superimposed on the XAFS spectrum. By comparing the responses of the IC, SPPD, and DD to the X-rays, nearly all the details can be found to have a one-to-one correspondence; however, the response ratio in pairs among the three detectors was only approximately linear, as shown in Fig. 4d. The slightly different responses of the detectors to the X-ray leads to minor deviations between the X-ray spectra or the XAFS curves recorded by the different detectors. Regardless, the IC-SPPD and DD-SPPD detector combinations for XAFS data acquisition remain feasible.

4.3 HF sampling XAFS data acquisition

In addition to the conventional XAFS measurement scheme, a new sampling scheme, HF sampling XAFS transmission, was tested when the beamstop-coupled SPPD was used as the rear detector. In the HF sampling scheme, the XAFS signals were collected in the transmission mode, and a high-speed counting module (NI 9223) was used for data collection. A high-speed counting module was used for the Cu K-edge XAFS measurements of the Cu foil at three sampling frequencies (1, 10, and 100 kHz). Here, the sampling frequency represents the number of times that an experimental signal (X-ray intensity) was repeatedly read in one second. Thus, the X-ray intensities in front and behind the sample were repeatedly read 10^3, 10^4, and 10^5 times per second at the three respective sampling frequencies. Note, the sampling rate of this high-speed counting card was higher than that (5000 data points/s) of IK220 [21]. A higher sampling rate can significantly improve data quality by raising the statistics.

For a typical XAFS spectrum covering an energy range of 1000 eV, the total measurement time of the XAFS spectrum in the HF sampling scheme was controlled within a few seconds (8 s) in the transmission mode at BSRF. Namely, each XAFS spectrum contains 8000, 80,000, and 800,000 data points under the three sampling frequencies. Figure 5a presents the raw Cu K-edge XAFS spectra of the Cu foil collected using the DD-SPPD detector combination at sampling frequencies of 1, 10, and 100 kHz. Note, the HF sampling XAFS data are clearly different than that of the conventional XAFS data in appearance. It is difficult to determine the data qualities and features from the raw HF sampling XAFS data. To save time, the XAFS data are usually recorded in chronological order (time dimension) in these HF sampling XAFS measurements. The XAFS data are required to be converted from the time domain into the energy space for a subsequent data analysis. Another important issue is that the HF sampling scheme does not increase the energy resolution of the XAFS spectra, however drastically increases the number of data points. Therefore, in addition to the abscissa transformation, an appropriate statistical average for the HF sampling XAFS data is necessary. Typically, for an XAFS spectrum covering an energy range of approximately 1000 eV, it is sufficient to retain a few hundred data points. Under 10^3, 10^4, or 10^5 sampling frequencies, the entire X-ray absorption spectrum recorded by the HF sampling scheme can be roughly divided into 800 time segments in chronological order. Each time segment had approximately 10, 100, or 1000 raw data points. These raw data points in each time segment must be summed and averaged to form one reduced data point. After data pre-processing, each XAFS spectrum was statistically averaged into 800 data points. Conservatively, this data preprocessing did not reduce the energy resolution. The 800 data points reserved for each XAFS spectrum were generally more than those for the traditional XAFS spectrum. The statistical average not only reduces the number of data points, but also significantly improves the SNR of the XAFS spectrum, as shown in Fig. 5b. Note, all three HF sampling XAFS spectra had 8 s data acquisition times; however, their SNRs after the statistical average preprocessing were different. For an energy region with a span smaller than the energy resolution, the XAFS signal can be regarded as approximately constant if the sampling frequency is sufficiently high. Therefore, the HF sampling scheme is equivalent to the repeated measurements of an approximately constant quantity and different sampling frequencies correspond to different repetitive measurement times. A higher sampling frequency leads to a greater statistic and lower noise. When the sampling frequency was as low as 1 kHz, the XAFS

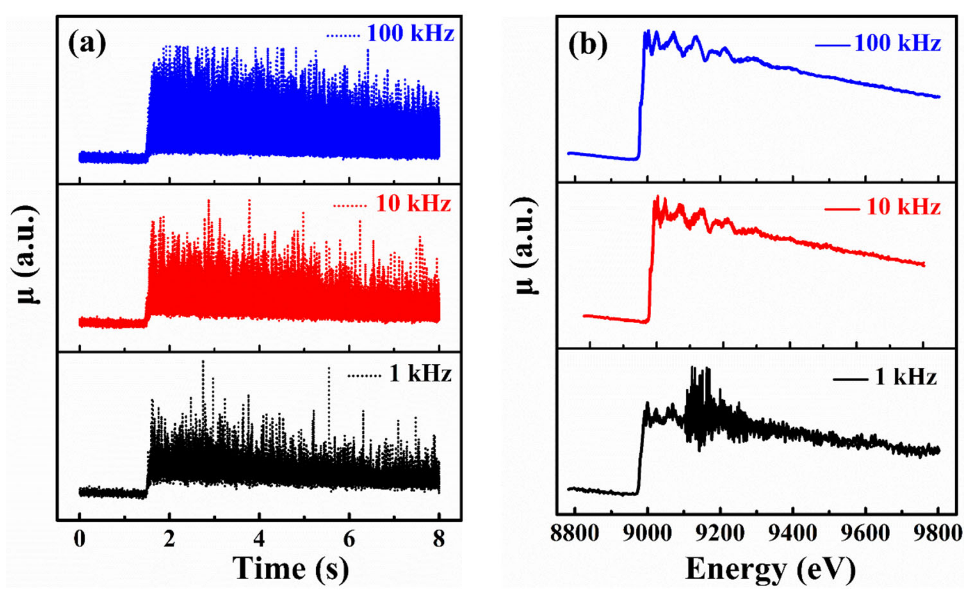

Fig. 5 (Color online) Cu-foil raw (**a**) and pre-processed (**b**) HF sampling XAFS spectra collected with the DD-SPPD detector combination at three sampling frequencies (from bottom to top: 1, 10, and 100 kHz)

spectrum after the statistical average remained too noisy, resulting in the failure of the XAFS spectrum, as shown in the curve at the bottom of Fig. 5b.

To convert the abscissa of the HF sampling XAFS spectra from chronological order (time domain) to the energy space, the absorption-edge position was first determined and marked as E_0, which corresponds to the first-derivative maximum of the XAFS spectrum. For a typical double-crystal monochromator, its rotation in the Bragg angle (θ) space is usually uniform. This indicates that the Bragg angle of the Si(111) monochromator linearly changed following the formula $\theta - \theta_0 = \omega\ (t - t_0)$. where θ_0 indicates the Bragg angle corresponding to the absorption edge of the element to be measured, t_0 is the time required for the monochromator to rotate to the absorption edge of the element, and ω is the rotation angular velocity of the monochromator. Based on the linear relationship between the Bragg angle (θ) and rotation time (t), the data point distribution of the HF sampling XAFS spectrum was also uniform in the Bragg angle space. The abscissa of the HF sampling XAFS spectra can be converted from the Bragg angle (θ) to the incident X-ray energy (E) using the following formula:

$$E(eV) = \frac{hc}{2d_{(111)}\sin\theta} = \frac{1977}{\sin\theta}, \tag{2}$$

where h is the Planck's constant (6.626×10^{-34} J·s), c is the velocity of light (2.998×10^{8} m·s^{-1}), and $d_{(111)}$ is the interplanar spacing of the Si(111) crystal plane (3.1357 Å). For the Cu foil sample, the absorption edge energy of the Cu K-edge (E_0) was 8979 eV. After reducing the number of data points and converting the abscissa to the energy space, the three XAFS spectra with sampling frequencies of 1, 10, and 100 kHz were also compared, as shown in Fig. 5b. Evidently, within the sampling frequency range of our investigation, a higher sampling frequency improved the data quality and SNR. This is because a higher sampling frequency indicates a greater number of measurements, thus improved statistical data.

4.4 Comparison of HF sampling XAFS spectra

To verify the data quality of the HF sampling XAFS spectra acquired by the SPPD, the Cu K-edge XAFS spectrum collected with the DD-SPPD detector combination and the 100 kHz sampling frequency was compared to the reference spectrum that was collected by the IC-IC detector combination in the conventional sampling mode. The E-space X-ray absorption spectra and k-space XAFS spectra of the Cu foil are shown in Fig. 6a, b, respectively, which demonstrates that regardless of the E-space or k-space, the HF sampling XAFS spectrum collected within a few seconds was very similar to the conventional XAFS spectrum collected within a few minutes, except for the fact that the SNR of the HF sampling XAFS spectrum was slightly worse. Considering the data with the IC-IC detector combination as a reference, the calculated Q factor was 0.017 for the X-ray absorption spectrum with the DD-SPPD detector combination shown in Fig. 6a, or 0.213 for the XAFS spectrum with the DD-SPPD detector combination shown in Fig. 6b. This result demonstrates that in addition to the SPPD detector being used for the collection of conventional XAFS spectra, it can also be used for the data acquisition of HF sampling XAFS. Furthermore, the Fourier transform spectra in the R-space and the isolated single-shell XAFS oscillations in the k-space were extracted, as shown in Fig. 6c, d, respectively. Similarly, the calculated Q factors were 0.121 and 0.068 for the Fourier transform spectrum and single-shell XAFS curve, respectively. Although the Q factor was defined in Eq. (1) to describe the similarity between the two curves, it was found that the calculated Q values were slightly different for the same data in the E-space, k-space, and R-space. Evidently, the Q-value calculated for the data in the k-space was the most sensitive to the curve deviation. A quantitative comparison between the HF-sampling and conventional XAFS spectra was also performed by fitting the nearest-neighbor single-shell XAFS oscillations of the Cu foil. The fitting curves are shown in Fig. 6c, d, and the fitting parameters are listed in Table 2.

The XAFS fitting results indicate that the fitting parameters of the nearest-neighbor structure are nearly the same for the 100 kHz HF sampling XAFS and conventional XAFS spectra. This study demonstrates that the SPPD is not only capable of being sufficiently applied for conventional XAFS measurements, but can also be sufficiently used for HF sampling XAFS measurements. The small size of the SPPD and ease of assembly with a beamstop makes it capable for use in a combined technique, including the XAFS measurement. The good performance of this SPPD in the HF sampling XAFS measurements proves that it can be sufficiently applied to time-resolved experimental measurements within seconds.

5 Conclusion

In this study, a commercial LSSPD-SPB3 silicon PIN photodiode was coupled in a beamstop to form a small detector. This detector was tested for conventional and HF-sampling XAFS data collection. By comparing the XAFS spectra collected with IC-IC and DD-SPPD detector combinations, the following conclusions can be drawn: (1) The SPPD detector sufficiently matches with a diamond-film detector, and the DD-SPPD detector combination can be used for XAFS data collection. (2) The SPPD as the rear

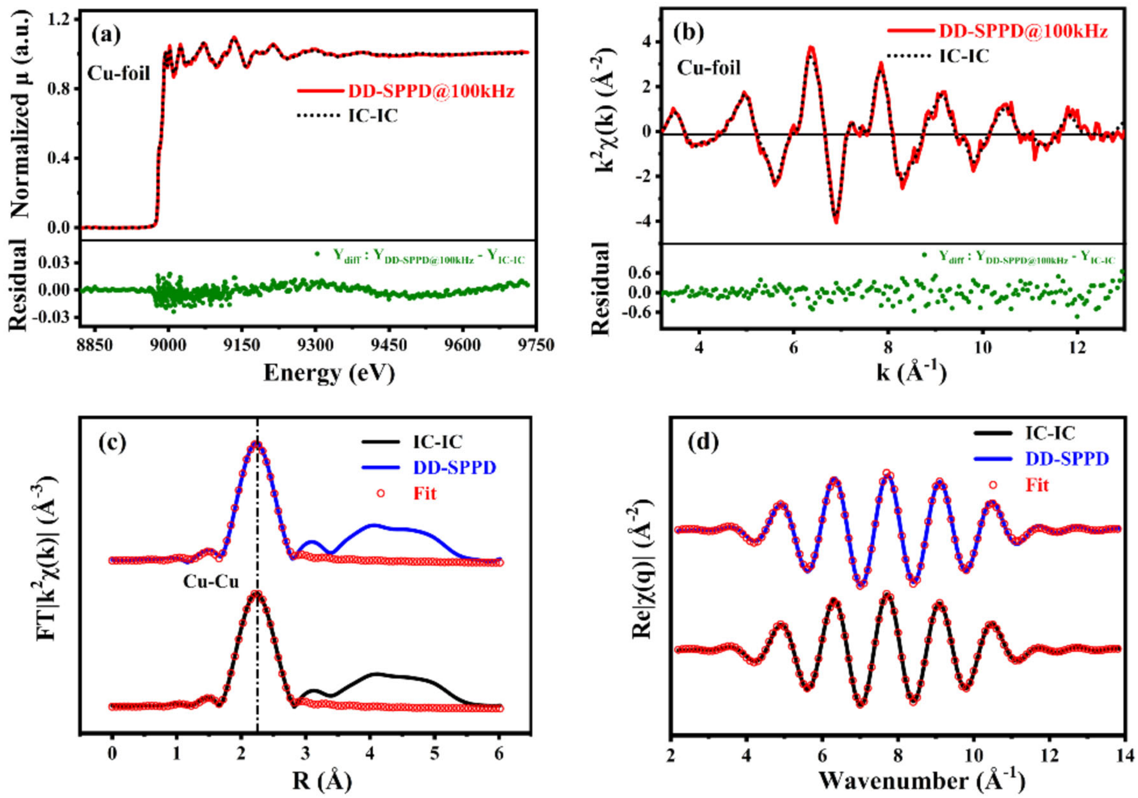

Fig. 6 (Color online) Comparison of Cu K-edge XAFS spectra of the Cu-foil between the HF sampling scheme (solid line) with the DD-SPPD detector combination, and the conventional scheme (dot line) with the IC-IC detector combination in the *E*-space (**a**) and *k*-space (**b**) as well as their differences. Comparison of the Fourier transform spectra (solid line) and the fitting curves (circle line) in the *R*-space (**c**) between the 100 kHz HF sampling XAFS mode with the DD-SPPD detector combination, and the conventional XAFS mode with the IC-IC detector combination, as well as a comparison between the isolated nearest-neighbor XAFS spectra (solid line) and the fitting curves (circle line) in the *k*-space (**d**) between the 100 kHz HF sampling XAFS mode with the DD-SPPD detector combination, and the conventional XAFS mode with the IC-IC detector combination

Table 2 Nearest-neighbor XAFS fitting parameters of the Cu foil for the XAFS spectra collected by the 100 kHz HF sampling XAFS mode with the DD-SPPD detector combination (DD-SPPD) and by the conventional XAFS mode with the IC-IC detector combination (IC-IC)

Sample	Bond	R (Å)	N	σ^2 ($\times$ 10^{-3} Å^2)	ΔE (eV)	R-factor ($\times$ 10^{-3})
Cu [28]	Cu–Cu	2.56	12	–	–	–
Cu foil (IC-IC)	Cu–Cu	2.54 $\pm$ 0.03	12.0 $\pm$ 0.6	8.8 $\pm$ 0.4	4.7 $\pm$ 0.6	1.7
Cu foil (DD-SPPD)	Cu–Cu	2.54 $\pm$ 0.05	12.0 $\pm$ 0.9	8.5 $\pm$ 0.6	4.5 $\pm$ 0.9	3.8

detector can be sufficiently used to collect data from conventional XAFS and HF sampling XAFS, verifying the feasibility of SPPD as the rear detector for XAFS acquisition. (3) The miniaturized SPPD detector is simple and convenient to use in a combined technique, including the XAFS measurement.

Author contributions All authors contributed to the study conception and design. Material preparation, data collection and analysis were performed by Yun-Peng Liu, Lei Yao and Bing-Jie Wang. The first draft of the manuscript was written by Yun-Peng Liu and all authors commented on previous versions of the manuscript. All authors read and approved the final manuscript.

References

1. Z. Sun, Q. Liu, T. Yao et al., X-ray absorption fine structure spectroscopy in nanomaterials. Sci. China Mater. **58**, 313–341 (2015). https://doi.org/10.1007/s40843-015-0043-4
2. M. Newville, Fundamentals of XAFS. Rev. Mineral. Geochem. **78**, 33–74 (2014). https://doi.org/10.2138/rmg.2014.78.2
3. X.P. Sun, F.F. Sun, S.Q. Gu et al., Local structural evolutions of CuO/ZnO/Al_2O_3 catalyst for methanol synthesis under operando conditions studied by in situ quick X-ray absorption

spectroscopy. Nucl. Sci. Teth. **28**, 21 (2017). https://doi.org/10.1007/s41365-016-0170-y
4. M. Luo, S.J. Deng, L. Li et al., XAFS and SRGI-XRD studies of the local structure of tellurium corrosion of Ni-18% Cr alloy. Nucl. Sci. Teth. **30**, 153 (2019). https://doi.org/10.1007/s41365-019-0673-4
5. L. Jiang, X.X. Ye, D.J. Wang et al., Synchrotron radiation-based materials characterization techniques shed light on molten salt reactor alloys. Nucl. Sci. Teth. **31**, 6 (2020). https://doi.org/10.1007/s41365-019-0719-7
6. K. Sato, Feasibility study of silicon PN photodiodes as X-ray intensity monitors for high flux X-ray beam with synchrotron radiation. Nucl. Instrum. Meth. A **436**, 285–290 (1999). https://doi.org/10.1016/S0168-9002(99)00635-X
7. G. Dalba, P. Fornasini, Y. Soldo et al., PIN silicon diodes as EXAFS signal detectors. J. Synchrotron Radiat. **3**, 213–219 (1996). https://doi.org/10.1107/S0909049596006073
8. E. Pace, A. De Sio, Z. Pan et al., Diamond photodetectors for X-ray absorption spectroscopy applications. AIP Conf. Proc. **1234**, 97–100 (2010). https://doi.org/10.1063/1.3463377
9. A.D. Sio, A. Bocci, E. Pace et al., Diamond solid state ionization chambers for X-ray absorption spectroscopy applications. Appl. Phys. Lett. **93**, 083503 (2008). https://doi.org/10.1063/1.2976125
10. B. Ravel, K. Attenkofer, J. Bohon et al., Diamond sensors and polycapillary lenses for X-ray absorption spectroscopy. Rev. Sci. Instrum. **84**, 103106 (2013). https://doi.org/10.1063/1.4824350
11. C. Storb, U. Dedek, W. Weber et al., Photodiodes as detectors with high dynamical range for X-ray reflectivity measurements. Nucl. Instrum. Meth. A **306**, 544–548 (1991). https://doi.org/10.1016/0168-9002(91)90050-Z
12. A. M. Beale, A.M.J.V.D. Eerden, S.D.M. Jacques et al., A combined SAXS/WAXS/XAFS setup capable of observing concurrent changes across the nano-to-micrometer size range in inorganic solid crystallization processes. J. Am. Chem. Soc. **128**, 12386–12387 (2006). https://doi.org/10.1021/ja062580r
13. A.J. Dent, G.N. Greaves, J.W. Couves et al., Combined x-ray absorption spectroscopy and X-ray powder diffraction. AIP Conf. Proc. **258**, 631–641 (1992). https://doi.org/10.1117/12.49471
14. S.N. Ehrlich, J.C. Hanson, A. Lopez et al., Combined XRD and XAS. Nucl. Instrum. Meth. A **649**, 213–215 (2011). https://doi.org/10.1016/j.nima.2010.11.07b
15. M.G. O'Brien, A.M. Beale, S.D.M. Jacques et al., A combined multi-technique in situ approach used to probe the stability of iron molybdate catalysts during redox cycling. Top Catal. **52**, 1400–1409 (2009). https://doi.org/10.1007/s11244-009-9324-z
16. C.E. Blanchet, C. Hermes, D.I. Svergun et al., A small and robust active beamstop for scattering experiments on high-brilliance undulator beamlines. J. Synchrotron Radiat. **22**, 461–464 (2015). https://doi.org/10.1107/S160057751402829X
17. R. Frahm, Quick scanning EXAFS: first experiments. Nucl. Instrum. Meth. A **270**, 578–581 (1988). https://doi.org/10.1016/0168-9002(88)90732-2
18. T. Uruga, H. Tanida, K. Kato et al., Improvement in XAFS beamline BL01B1 at SPring-8. J. Phys. Conf. Ser. **190**, 012041 (2009). https://doi.org/10.1088/1742-6596/190/1/012041
19. C. Prestipino, O. Mathon, R. Hino et al., Quick-EXAFS implementation on the general purpose EXAFS beamline at ESRF. J. Synchrotron Radiat. **18**, 176–182 (2011). https://doi.org/10.1107/S0909049510046546
20. H.S. Yu, X.J. Wei, J. Li et al., The XAFS beamline of SSRF. Nucl. Sci. Teth. **26**, 050102 (2015), https://doi.org/10.13538/j.1001-8042/nst.26.050102
21. S. Khalid, W. Caliebe, P. Siddons et al., Quick extended X-ray absorption fine structure instrument with millisecond time scale, optimized for in situ applications. Rev. Sci. Instrum. **81**, 015105 (2010). https://doi.org/10.1063/1.3276679
22. H. Liu, Y. Zhou, S. Gu et al., Data acquisition system modified by IK220 card for the SSRF XAFS station. Nucl. Tech. **35**, 561–567 (2012). https://doi.org/10.1007/s11783-011-0280-z
23. L. Yao, Y. Liu, B. Wang et al., A polycrystalline diamond micro-detector for X-ray absorption fine-structure measurements. J. Synchrotron Radiat. **29**, 424–430 (2022). https://doi.org/10.1107/S1600577521013011
24. M. Kocsis, A. Somogyi, Miniature ionization chamber detector developed for X-ray microprobe measurements. J. Synchrotron Radiat. **10**, 187–190 (2003). https://doi.org/10.1107/S0909049502019854
25. Y. Dong, W. Wang, D. Lei et al., Suppression of dark current in germanium-tin on silicon pin photodiode by a silicon surface passivation technique. Opt. Express **23**, 18611–18619 (2015). https://doi.org/10.1364/OE.23.018611
26. S. Su, B. Cheng, C. Xue et al., GeSn p-i-n photodetector for all telecommunication bands detection. Opt. Express **19**, 6400–6405 (2011). https://doi.org/10.1364/OE.19.006400
27. B. Ravel, M. Newville, ATHENA, ARTEMIS, HEPHAESTUS: data analysis for X-ray absorption spectroscopy using IFEFFIT. J. Synchrotron Radiat. **12**, 537–541 (2005). https://doi.org/10.1107/S0909049505012719
28. I.K. Suh, H. Ohta, Y. Waseda, High-temperature thermal expansion of six metallic elements measured by dilatation method and X-ray diffraction. J. Mater. Sci. **23**, 757–760 (1988). https://doi.org/10.1007/BF01174717